Check for updates

PHYSIOLOGY

Neuronal GPR75 deficiency protects against diet-induced obesity in a humanized mouse model

Xue-Nan Sun[1]†, Jan-Bernd Funcke[1]†, Chanmin Joung[1], Chao Li[1], Ayanna Cobb[1], Toshiharu Onodera[1,2], Joselin Velasco[1], May-Yun Wang[1], Patrick Joseph Antonellis[3], Christopher Mazzone[3], Jared Senfeld[3], Minrong Ai[3], Philipp E. Scherer[1], Da Young Oh[1]*

Copyright © 2026 The Authors, some rights reserved; exclusive licensee American Association for the Advancement of Science. No claim to original U.S. Government Works. Distributed under a Creative Commons Attribution NonCommercial License 4.0 (CC BY-NC).

GPR75, a G protein–coupled receptor implicated in human obesity through loss-of-function variants, has emerged as a promising regulator of energy and metabolic homeostasis. To dissect its tissue-specific functions, we generated a humanized floxed *Gpr75* mouse model with conditional deletions in the brain and adipose tissue. Mice with brain-specific Gpr75 deletion using Nestin-Cre were resistant to diet-induced obesity, primarily through suppressed food intake and modest increases in energy expenditure. In contrast, adipocyte-specific deletion of Gpr75 had minimal effects on systemic metabolism but modestly enhanced mitochondrial oxygen consumption in brown adipose tissue under cold exposure. Gpr75 expression was up-regulated in key brain regions and down-regulated in white adipose tissue under high-fat diet conditions, supporting a predominant central role in metabolic adaptation. Histological and transcriptomic analyses further revealed depot-specific effects on adipocyte morphology and hepatic lipid accumulation in global knockouts. These findings position GPR75 as a critical regulator of central energy balance and provide a mechanistic framework for developing brain-targeted therapies against obesity.

INTRODUCTION

Obesity and its associated metabolic complications, including insulin resistance and type 2 diabetes, continue to present major public health challenges worldwide (*1*, *2*). Despite advances in understanding the genetic and physiological factors contributing to obesity, the mechanistic underpinnings of how specific genes and signaling pathways regulate body weight and metabolic homeostasis remain incompletely defined (*3*–*5*). Recent human genetic studies have highlighted G protein–coupled receptor 75 (GPR75) as a potential modulator of obesity risk (*6*–*8*). Loss-of-function variants in the GPR75 gene are associated with protection against obesity and improved metabolic profiles, suggesting that GPR75 may act as a regulator of body weight, energy balance, and glucose homeostasis (*7*, *9*, *10*). Mouse studies have supported these findings, as whole-body deletion of Gpr75 leads to a lean phenotype and improved glucose tolerance (*7*, *11*). However, the precise tissues and mechanisms through which GPR75 exerts its metabolic effects remain unclear.

GPR75 is a class A G protein–coupled receptor (GPCR) with predominant expression in the central nervous system (*12*), including the hypothalamus and brainstem, areas that are critical for appetite regulation and energy expenditure (*13*, *14*). It is also expressed at lower levels in peripheral metabolic tissues such as white and brown adipose tissue (BAT) (*11*). While GPR75 has been proposed to couple to the G_q-mediated pathway and respond to 20-hydroxyeicosatetraenoic acid (20-HETE), its endogenous ligands, tissue-specific roles, and downstream effectors remain largely undefined (*15*, *16*).

To dissect the physiological relevance and tissue-specific actions of GPR75 in metabolic regulation, we developed a humanized floxed *Gpr75* (*hGpr75*$^{fl/fl}$) mouse model and performed targeted deletions in brain and adipose tissues (*10*, *16*). We investigated how GPR75 signaling in these compartments influences food intake, energy expenditure, glucose homeostasis, and thermogenic responses under both basal and stress conditions such as high-fat diet (HFD) feeding and cold exposure. These studies aim to clarify the contributions of central and peripheral GPR75 signaling to systemic energy balance and to evaluate its potential as a therapeutic target for obesity and metabolic disease.

RESULTS

Gpr75 transcription patterns in mouse, rat, and monkey brains

To investigate the cellular identity of Gpr75-expressing cells in metabolically relevant brain regions, we first performed multiplexed error-robust fluorescence in situ hybridization (MERFISH) on coronal sections of mouse hypothalamus and dorsal vagal complex (DVC). Consistent with previous reports (*16*, *17*), Gpr75 mRNA was broadly distributed across both regions (Fig. 1). Most Gpr75-expressing cells coexpressed Solute Carrier Family 32 Member 1 (*Slc32a1*), a marker of GABAergic neurons, or *Slc17a6*, a glutamatergic marker (Fig. 1, A, C, D, and F), indicating that Gpr75 is primarily expressed in neurons. We also observed partial overlap of Gpr75 with neuropeptide and receptor genes involved in energy balance, including glucagon-like peptide-1 receptor (*Glp1r*), gastric inhibitory polypeptide receptor (*Gipr*), calcitonin receptor (*Calcr*), and tyrosine hydroxylase (*Th*) in both hypothalamus and DVC (Fig. 1). Analysis of specific neuronal populations revealed that Gpr75 is not enriched in any single cell type but is present in ~30 to 50% of multiple neuronal subtypes, including agouti-related peptide (*Agrp*)$^+$, proopiomelanocortin (*Pomc*)$^+$, GDNF family receptor alpha-like (*Gfral*)$^+$, and choline acetyltransferase (*Chat*)$^+$ cells (Fig. 1, B to F). These findings support the hypothesis

[1]Touchstone Diabetes Center, University of Texas Southwestern Medical Center, Dallas, TX 75390, USA. [2]Department of Adipose Management, Graduate School of Medicine, The University of Osaka, Suita, Osaka, Japan. [3]Eli Lilly Research Laboratories, Division of Eli Lilly and Company, Indianapolis, IN 46285, USA.
*Corresponding author. Email: dayoung.oh@utsouthwestern.edu
†These authors contributed equally to this work.

Downloaded from https://www.science.org at University of Texas Southwestern Medical Center on January 24, 2026

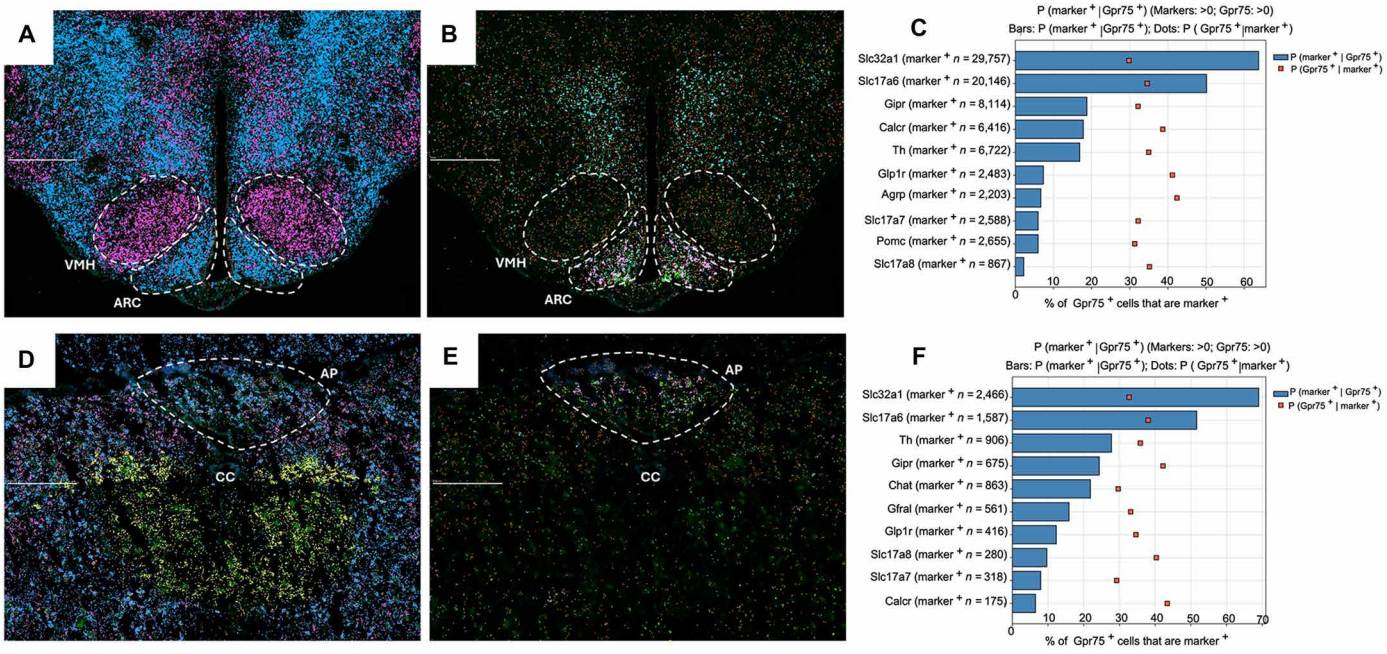

Fig. 1. Gpr75 mRNA expression in mouse hypothalamus and DVC. MERFISH was performed on coronally sectioned mouse hypothalamus [(A) and (B)] and DVC [(D) and (E)]. (**A**) Representative MERFISH images showing expression of *Gpr75* (orange), *Slc32a1* (blue), and *Slc17a6* (purple) in the hypothalamus. (**B**) Expression of *Gpr75* (orange), *Calcr* (cyan), *Agrp* (green), and *Pomc* (pink) in the hypothalamus. (**C**) Quantification of hypothalamic coexpression: Bar graphs show the percentage of $Gpr75^{+}$ cells that coexpress each marker gene (blue bars), and orange dots represent the percentage of marker-positive cells that coexpress *Gpr75*. (**D**) Representative images showing *Gpr75* (orange), *Slc32a1* (blue), *Slc17a6* (purple), and *Chat* (yellow) in the DVC. (**E**) Expression of *Gpr75* (orange), *Calcr* (cyan), *Glp1r* (green), and *Gipr* (pink) in the DVC. (**F**) Quantification of DVC coexpression using the same scheme as in (C), with $Gpr75^{+}$ cells shown as blue bars and marker-positive cells coexpressing *Gpr75* as orange dots. Scale bars, 1 mm [(A) and (B)]; 0.5 mm [(D) and (E)]. VMH, ventral medial hypothalamus; ARC, arcuate nucleus of hypothalamus; CC, central canal.

that Gpr75 may function in diverse neural circuits implicated in feeding and metabolic regulation.

To assess whether this broad neural expression pattern is evolutionarily conserved, we performed Gpr75-specific RNA in situ hybridization (ISH; RNAscope) on sagittal brain sections from mice, rats, and cynomolgus monkeys. In mice, Gpr75 was widely expressed in the cortex, hypothalamus, hippocampus, area postrema (AP), and cerebellum (fig. S1A). Rats exhibited a nearly identical distribution (fig. S1B), and cynomolgus monkeys similarly showed widespread GPR75 expression (fig. S1C). In the monkey cerebellum, GPR75 was more restricted to the surface of the granule cell layer (fig. S1C; r − r1), whereas in mice and rats, Gpr75 expression was more evenly distributed throughout this layer (fig. S1, A and B; f − f1, l − l1). Together, these findings demonstrate that Gpr75 is broadly expressed across neuronal subtypes in metabolically relevant regions of the brain and that this expression pattern is conserved across mouse, rat, and monkey brains with minor species-specific differences.

Generation of $hGpr75^{fl/fl}$ mice

To enable compound screening and dissect the systemic functions of GPR75, we generated a humanized, conditional knockout (KO) mouse model using CRISPR-Cas9 genome editing to modify the endogenous *Gpr75* locus on mouse chromosome 11 (ENSMUSG00000043999). The mouse *Gpr75* gene contains two exons, with the full coding sequence (open reading frame, ORF) located in exon 2 and regulated by distinct promoter (Pro) and polyadenylation (pA) elements (Fig. 2A). We replaced the murine ORF with the human GPR75 coding sequence, while retaining the native mouse 5′ and 3′ untranslated regions (UTRs) to preserve physiological transcriptional regulation. In addition, loxP sites were inserted into evolutionarily nonconserved regions within intron 1 and the 3′ UTR, allowing for Cre-mediated deletion of the human *GPR75* ORF (Fig. 2A). This strategy generated a floxed, humanized *Gpr75* allele ($hGpr75^{fl/fl}$), which expresses human GPR75 in place of the endogenous mouse protein, while maintaining the genomic architecture of the locus. This humanized mouse model serves as a versatile platform for in vivo tissue-specific or inducible deletion of *GPR75* by crossing with appropriate Cre-driver lines. It also provides a physiologically relevant system for translational studies aimed at targeting human GPR75.

Whole-body Gpr75 deletion reduces obesity and improves metabolic health in HFD-fed mice

Given previous reports that global *Gpr75* KO mice are resistant to HFD-induced obesity (*7*), we first assessed the role of GPR75 in diet-induced weight gain and metabolic dysfunction. To this end, we generated systemic Gpr75 KO mice ($Gpr75^{KO/KO}$) by crossing $hGpr75^{fl/fl}$ mice with cytomegalovirus-Cre mice. Successful recombination of the $hGpr75^{fl/fl}$ allele was confirmed in tail DNA from $Gpr75^{KO/KO}$ mice but not in $hGpr75^{fl/fl}$ or wild-type controls ($Gpr75^{wt/wt}$) (fig. S2, A and B). When challenged with an HFD, male $Gpr75^{KO/KO}$ mice exhibited significantly reduced weight gain compared to all other genotypes, with divergence in body weight emerging early during HFD feeding (Fig. 2B). Body composition analysis revealed a marked reduction in fat mass in $Gpr75^{KO/KO}$ mice, with no noticeable difference in lean mass relative to $Gpr75^{wt/wt}$ controls (Fig. 2C). Additionally, food intake was notably lower in $Gpr75^{KO/KO}$ mice after

Downloaded from https://www.science.org at University of Texas Southwestern Medical Center on January 24, 2026

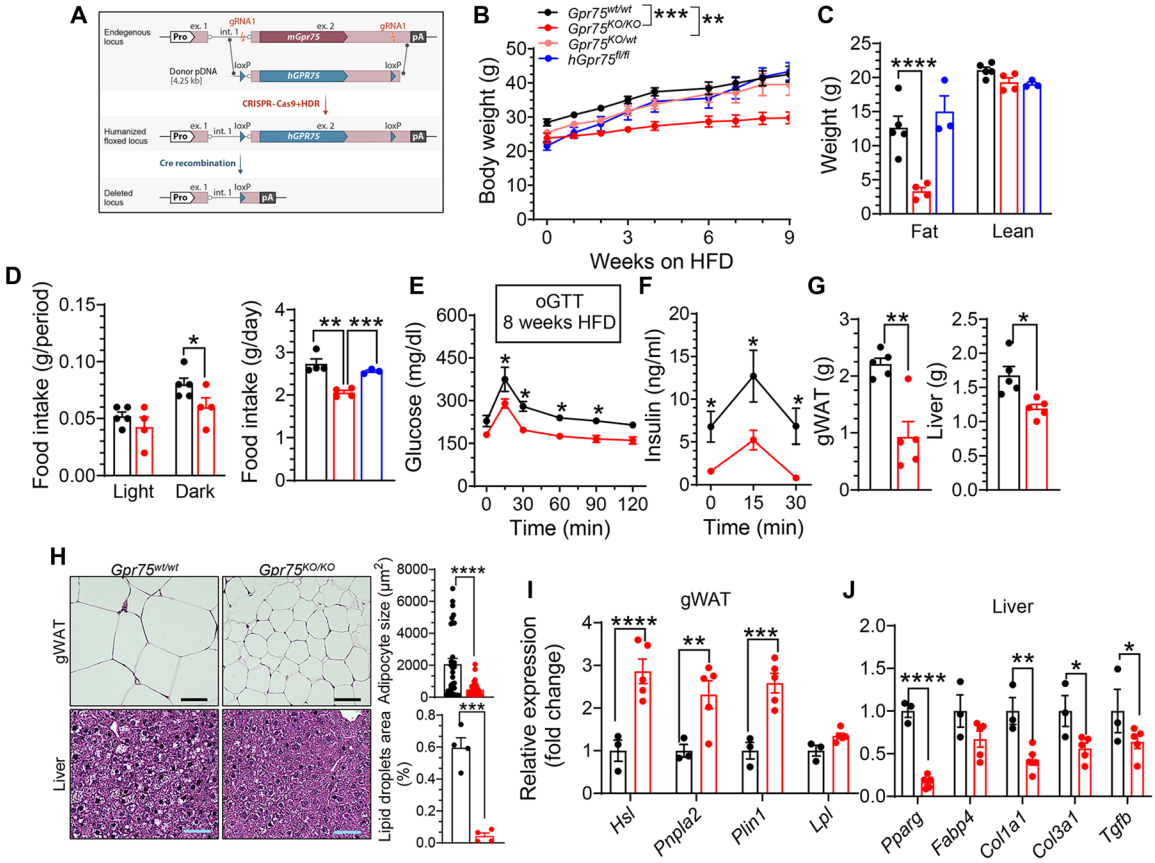

Fig. 2. Generation of *hGpr75*$^{fl/fl}$ mice and phenotype of whole-body *Gpr75* KO mice. (**A**) Schematic overview of mouse line generation. (**B**) Body weight of male *Gpr75*$^{wt/wt}$, *Gpr75*$^{KO/KO}$, *Gpr75*$^{KO/wt}$, and *hGpr75*$^{fl/fl}$ mice during HFD feeding ($n = 4$ to 5 per group). (**C**) Body composition after 2 months of HFD feeding ($n = 4$ to 5 per group). (**D**) Food intake measured after 2 months of HFD feeding ($n = 4$ to 5 per group). (**E** and **F**) Blood glucose (E) and serum insulin (F) levels during an oral glucose tolerance test (oGTT) after 2 months of HFD feeding ($n = 4$ to 5 per group). (**G**) gWAT and liver weights after 2 months of HFD feeding ($n = 4$ to 5 per group). (**H**) Representative H&E-stained images of gWAT and liver tissues after 2 months of HFD feeding. Scale bars, 50 μm. (**I**) RT-qPCR analysis of lipolysis-related gene expression in gWAT ($n = 3$ to 5 per group). (**J**) RT-qPCR analysis of fibrosis-related gene expression in liver ($n = 3$ to 5 per group). Data are presented as means ± SEM. Statistical analysis was performed using a two-tailed Student's *t* test [(C) and (D)] or two-way analysis of variance (ANOVA) with Bonferroni's multiple comparisons test [(B), (E), and (F)]. *$P < 0.05$; **$P < 0.01$; ***$P < 0.001$; ****$P < 0.0001$.

2 months of HFD feeding (Fig. 2D). To determine whether changes in energy expenditure contributed to the lean phenotype, we performed metabolic cage studies after 8 weeks of HFD feeding. No substantial differences were detected in oxygen (O_2) consumption, carbon dioxide (CO_2) production, respiratory exchange ratio (RER), heat production, or locomotor activity (fig. S3), suggesting that reduced food intake is the primary driver of the observed phenotype. Despite this, *Gpr75*$^{KO/KO}$ mice exhibited markedly improved glucose tolerance and insulin sensitivity compared to *Gpr75*$^{wt/wt}$ controls (Fig. 2, E and F). Histological analysis using hematoxylin and eosin (H&E) staining revealed reduced adipocyte sizes in gonadal white adipose tissue (gWAT) from *Gpr75*$^{KO/KO}$ mice (Fig. 2, G and H). Consistent with this, expression of genes involved in lipolysis, including *Hsl*, *Pnpla2*, *Plin1*, and *Lpl*, was drastically up-regulated in gWAT (Fig. 2I), suggesting enhanced lipid mobilization. H&E staining of liver tissue revealed decreased hepatic lipid accumulation in *Gpr75*$^{KO/KO}$ mice (Fig. 2H). Reverse transcription quantitative polymerase chain reaction (RT-qPCR) analysis confirmed a noticeable reduction in expression of fibrotic markers (*Col1a1*, *Col2a1*, *Tgfb*, and *Ccn2*/*Ctgf*) in the liver function (Fig. 2J), suggesting improved hepatic health. We observed similar protective effects in female *Gpr75*$^{KO/KO}$ mice, which showed reduced fat accumulation, lower food intake, and improved glucose and insulin responses compared to *Gpr75*$^{wt/wt}$ controls (fig. S4, A to F). Notably, under regular chow diet conditions, *Gpr75*$^{KO/KO}$ and control mice showed no dramatic differences in body weight, food intake, adiposity, or glucose tolerance (fig. S4, G to J), with only a modest difference in insulin sensitivity at 20 weeks of age (fig. S4K). Together, these findings demonstrate that while *Gpr75* deletion has minimal metabolic effects under basal chow-fed conditions, loss of GPR75 confers strong protection against HFD-induced obesity and metabolic dysfunction in both male and female mice. These results support a key role for GPR75 in regulating energy balance and metabolic health under obesogenic stress.

Deletion of hGpr75 in the brain is sufficient to protect mice from HFD-induced obesity

To investigate the specific contribution of GPR75 signaling in the nervous system to the metabolic phenotype observed in systemic *Gpr75*$^{KO/KO}$ mice, we generated brain-specific Gpr75 KO mice (*hGpr75*^{NKO}) by crossing *hGpr75*$^{fl/fl}$ with *Nestin-Cre* transgenic

Downloaded from https://www.science.org at University of Texas Southwestern Medical Center on January 24, 2026

mice (Fig. 3A). Nestin-Cre drives recombination in neural progenitors that give rise to both neurons and glia cells (*18*). RT-qPCR confirmed ~85% reduction of hGpr75 mRNA in the hypothalamus and ~90% reduction in the pons of $hGpr75^{NKO}$ mice relative to $hGpr75^{fl/fl}$ controls (fig. S5A). As designed, mouse *Gpr75* was absent in both genotypes due to humanization of the allele. RNA ISH confirmed robust *hGPR75* expression in the hypothalamus and AP, which was considerably diminished in $hGpr75^{NKO}$ mice (fig. S5, B to E).

Under the chow-fed conditions at 20 weeks of age, $hGpr75^{NKO}$ mice exhibited increased fat mass and reduced lean mass compared to controls (fig. S5, F to H), although body weight, food intake, glucose tolerance, and insulin sensitivity were not dramatically different (fig. S5, I and J). Following HFD challenge, male $hGpr75^{NKO}$ mice displayed notably reduced body weight and food intake compared to controls (Fig. 3, B to D). Indirect calorimetry revealed modest increases in O_2 consumption, CO_2 production, and heat generation during the light phase, whereas no differences were observed during the dark phase (fig. S6, A, B, C, E, and F). RER and locomotor activity remained unchanged (fig. S6, D, G, and H). These data suggest a mild increase in energy expenditure, with reduced food intake likely being the dominant contributor to the lean phenotype (*19*). $hGpr75^{NKO}$ mice exhibited improved glucose tolerance and insulin sensitivity following 8 weeks of HFD feeding (Fig. 3, E to G). Liver and BAT weights were dramatically decreased, whereas inguinal white adipose tissue (iWAT) was unchanged, and gWAT showed a modest increase (fig. S7, A to E). Histological analysis revealed reduced lipid accumulation in the liver (Fig. 3H, right-hand side), and RT-qPCR analyses showed markedly lower expression of fibrosis markers including *Col1a1*, *Col2a1*, *Ccn2* (*Ctgf*), and *Tgfb* (Fig. 3I), indicating protection against HFD-induced hepatic fibrosis.

These findings demonstrate that brain-specific deletion of GPR75 is sufficient to protect HFD-induced obesity and associated metabolic dysfunction. The protective phenotype appears to arise from both decreased food intake and a modest increase in energy expenditure, supporting the hypothesis that the lean phenotype in whole-body $Gpr75^{KO/KO}$ mice is primarily driven by loss of GPR75 signaling in Nestin-Cre-expressing brain cells.

Deficiency of hGpr75 in adipocytes does not protect mice from HFD-induced obesity or metabolic dysfunction

To assess the contribution of adipocyte-specific GPR75 signaling to the metabolic phenotype observed in systemic Gpr75 KO mice, we generated adipocyte-specific KO mice ($hGpr75^{AKO}$) by crossing $hGpr75^{fl/fl}$ mice with adiponectin-Cre transgenic mice (Fig. 4A).

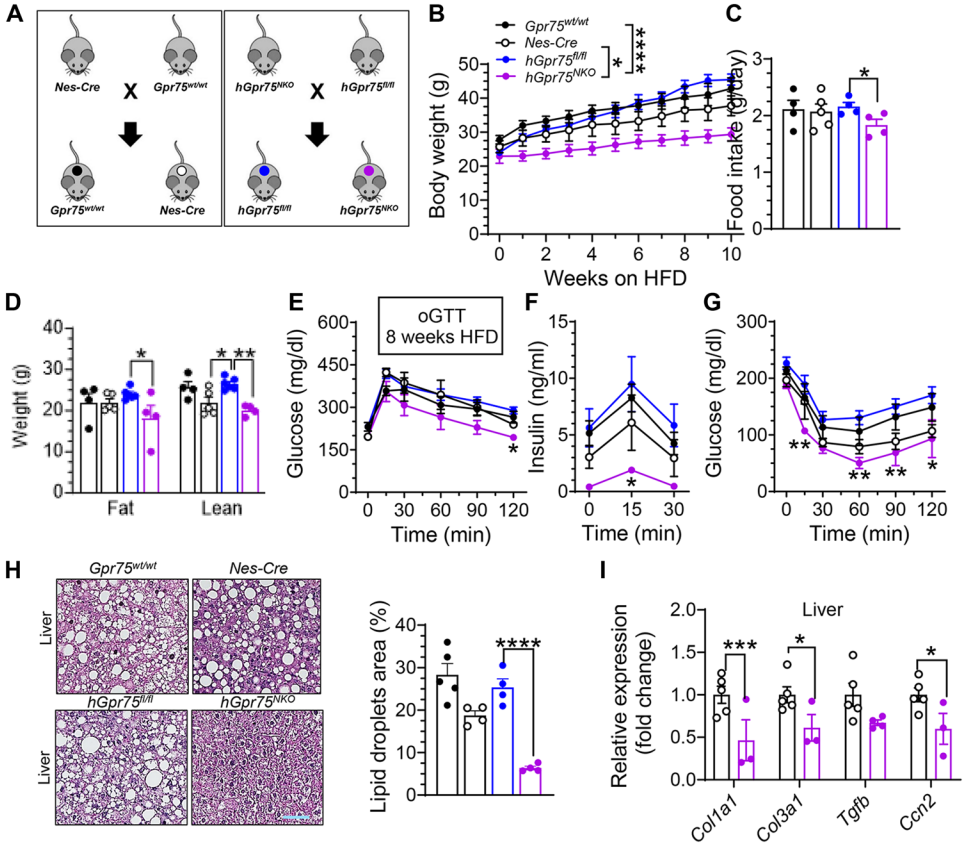

Fig. 3. Deletion of *hGpr75* in central and peripheral neurons is sufficient to protect mice from HFD-induced obesity. (**A**) Breeding scheme for the generation of $Gpr75^{wt/wt}$, *Nes-Cre*, $hGpr75^{fl/fl}$, and $hGpr75^{NKO}$ mice. (**B**) Body weight of male mice during HFD feeding ($n = 3$ to 5 per group). (**C**) Food intake measured after 5 weeks of HFD feeding ($n = 3$ to 5 per group). (**D**) Body composition after 12 weeks HFD feeding ($n = 4$ to 9 per group). (**E** and **F**) Blood glucose (E) and serum insulin (F) levels during an oGTT after 2 months of HFD feeding ($n = 3$ to 5 per group). (**G**) Blood glucose levels during intraperitoneal insulin tolerance test (ipITT) after 2 months of HFD feeding ($n = 3$ to 5 per group). (**H**) Representative H&E-stained liver sections after 5 months of HFD feeding. Scale bar, 50 μm. (**I**) RT-qPCR analysis of fibrosis-related gene expression in liver after 5 months of HFD feeding ($n = 3$ to 5 per group). Data are presented as means ± SEM. Statistical analysis was performed using a two-tailed Student's *t* test [(C), (D), and (I)] or two-way ANOVA with Bonferroni's multiple comparisons test [(B), (E), and (G)]. $^*P < 0.05$; $^{**}P < 0.01$; $^{***}P < 0.001$; $^{****}P < 0.0001$.

Downloaded from https://www.science.org at University of Texas Southwestern Medical Center on January 24, 2026

Efficient deletion of *hGpr75* was confirmed specifically in adipocytes through qPCR analyses of both whole adipose tissue and isolated adipocyte fractions (fig. S8, A to D). Under the HFD condition, male *hGpr75*^{AKO} mice exhibited no considerable differences in body weight gain, body composition, glucose tolerance, or insulin sensitivity compared to *hGpr75*$^{fl/fl}$ controls (Fig. 4, B to F). These results were consistent under chow-fed conditions as well (fig. S8, E to K), indicating that GPR75 deletion in adipocytes does not affect systemic metabolism under either dietary regimen. Given the reduced adipocyte size and elevated lipolysis gene expression observed in the gWAT of *Gpr75*$^{KO/KO}$ mice, we further assessed lipid metabolism in *hGpr75*^{AKO} mice using an oral triglyceride clearance (oTGC) test. There were no remarkable differences in circulating triglyceride (TG), nonesterified fatty acid (NEFA), or glycerol levels between *hGpr75*^{AKO} and control mice (Fig. 4, G to I), suggesting that lipid uptake and disposal were unaffected by adipocyte-specific GPR75 deficiency. Together, these findings indicate that GPR75 signaling in adipocytes does not play a major role in regulating energy balance or protecting against HFD-induced metabolic dysfunction. The absence of a phenotype in *hGpr75*^{AKO} mice, in contrast to the marked protection observed in whole-body and brain-specific KO models, supports the conclusion that the metabolic benefits of Gpr75 deletion are primarily mediated through the central nervous system rather than through adipose tissue.

Elimination of hGpr75 from adipocytes confers augmented cold tolerance in chow-fed mice

Although no metabolic differences were observed between *hGpr75*^{AKO} and *hGpr75*$^{fl/fl}$ mice under HFD conditions, a noticeable difference in thermoregulation emerged during acute cold exposure. Specifically, after a 5-hour cold challenge, *hGpr75*^{AKO} mice maintained a higher core body temperature compared to *hGpr75*$^{fl/fl}$ controls (Fig. 5, A and B). Because acute cold exposure typically stimulates glucose and lipid catabolism, we also monitored blood glucose levels and body weight during this period but found no noteworthy differences between groups (Fig. 5, C to E). Given prior reports that global *Gpr75*$^{KO/KO}$ mice exhibit increased thermogenesis in adipose tissue (*6*–*8*), we next asked whether chronic cold exposure would amplify these effects in *hGpr75*^{AKO} mice. However, after 5 days of cold exposure, no sustained differences in core body temperature were observed between *hGpr75*^{AKO} and *hGpr75*$^{fl/fl}$ mice (Fig. 5F).

Because acute cold exposure engages both shivering and nonshivering thermogenesis, we assessed mitochondrial function by measuring the O_2 consumption rate (OCR) in BAT and iWAT explants. Following cold exposure, BAT explants from *hGpr75*^{AKO} mice exhibited ~25% higher OCR compared to those from *hGpr75*$^{fl/fl}$ controls (Fig. 5G). In contrast, no substantial differences in OCR or thermogenic/beiging gene expression were detected in iWAT or gWAT between genotypes (fig. S9, A to D). These findings suggest that adipocyte-specific deletion of GPR75 modestly enhances cold-induced mitochondrial activity in BAT, despite having no detectable impact on systemic metabolic phenotypes under HFD condition. While the overall role of adipocyte GPR75 signaling appears limited, these results raise the possibility that it may play a minor role in regulating thermogenic capacity, potentially via subtle modulation of mitochondrial function or cold sensitivity.

DISCUSSION

This study establishes GPR75 as a key regulator of obesity and metabolic homeostasis, with distinct contributions from brain and adipocyte signaling pathways. Using *hGpr75*$^{fl/fl}$ mice, we dissected tissue-specific roles of GPR75 and found that it plays a predominant role in the central regulation of energy balance, with a modest and context-dependent influence on adipose tissue thermogenesis.

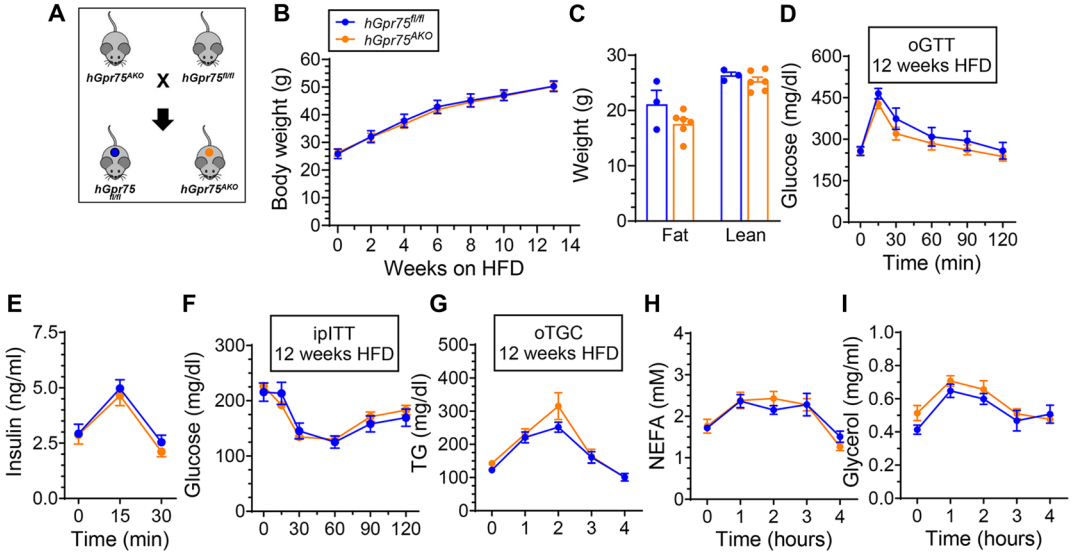

Fig. 4. Adipocyte-specific *hGpr75* deficiency does not protect mice from HFD-induced obesity or metabolic deterioration. (**A**) Breeding scheme for the generation of *hGpr75*$^{fl/fl}$ and *hGpr75*^{AKO} mice. (**B**) Body weight of male mice during HFD feeding ($n = 5$ to 9 per group). (**C**) Body composition after 2 months of HFD feeding ($n = 4$ to 5 per group). (**D** and **E**) Blood glucose (D) and serum insulin (E) levels during an oGTT after 2 months of HFD feeding ($n = 5$ to 9 per group). (**F**) Blood glucose levels during ipITT after 2 months of HFD feeding ($n = 5$ to 9 per group). (**G** to **I**) Serum levels of TG (G), NEFA (H), and glycerol (I) during an oTGC test after 2 months of HFD feeding ($n = 5$ to 9 per group). Data are presented as means ± SEM. Statistical analysis was performed using a two-tailed Student's *t* test (C) or two-way ANOVA with Bonferroni's multiple comparisons test [(B) and (D) to (I)].

Downloaded from https://www.science.org at University of Texas Southwestern Medical Center on January 24, 2026

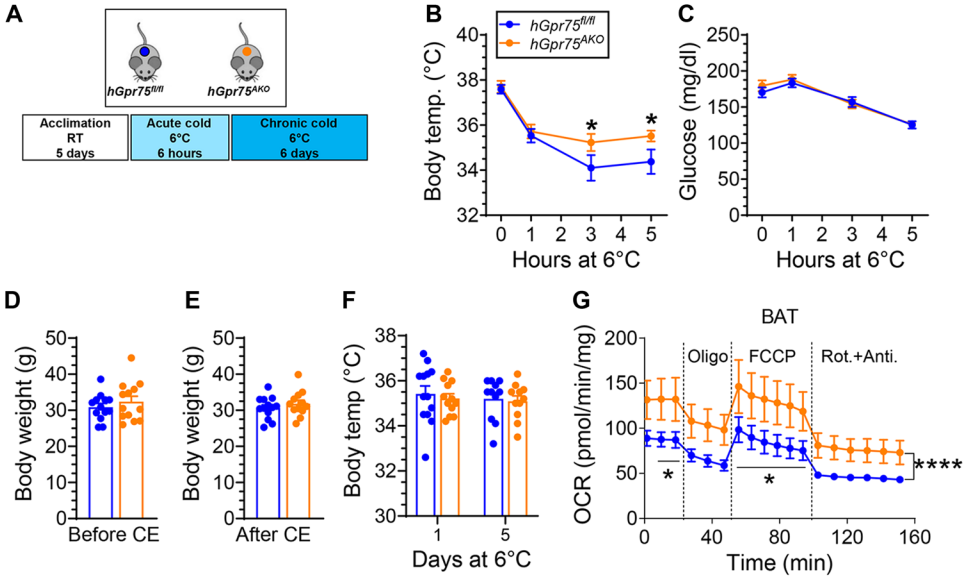

Fig. 5. Adipocyte-specific *hGpr75* deletion enhances cold tolerance in chow-fed mice. (**A**) Experimental design for acute and chronic cold exposure of *hGpr75*$^{fl/fl}$ and *hGpr75*^{AKO} mice. (**B** and **C**) Core body temperature (B) and blood glucose levels (C) measured during acute cold exposure ($n = 5$ to 9 per group). (**D** and **E**) Body weight before (D) and after (E) acute cold exposure (CE) ($n = 5$ to 9 per group). (**F**) Core body temperature during chronic cold exposure ($n = 5$ to 9 per group). (**G**) OCR of BAT explants measured by Seahorse analysis after 5 hours of acute cold exposure ($n = 5$ per group). Data are presented as means ± SEM. Statistical analysis was performed using a two-tailed Student's *t* test [(D), (E), and (F)] or two-way ANOVA with Bonferroni's multiple comparisons test [(B), (C), and (G)]. *$P < 0.05$; ****$P < 0.0001$.

Consistent with previous studies, we confirmed that *Gpr75* expression is broadly expressed in the brain (*8*, *11*), including the hypothalamus and AP (*12*). These regions are known to be integral to appetite and energy balance regulation (*20*, *21*). This widespread neural expression contrasts with other adiposity-related genes such as *Agrp* (*22*) and *Pomc* (*23*), which are confined to specific neuronal subpopulations (*23*–*25*). The broader distribution suggests that GPR75 may have a wider regulatory role (*26*). Deletion of *Gpr75* in the brain reduced food intake and modestly increased energy expenditure, reinforcing its central function in energy homeostasis. Although both whole-body and brain-specific Gpr75 KO models showed lean phenotypes, the relative contributions differed. In systemic *Gpr75*$^{KO/KO}$ mice, reduced food intake was the main driver of the lean phenotype, possibly reflecting both central and peripheral effects. In the Nestin-Cre model, which deletes Gpr75 in neural progenitors affecting neurons and glia in both central peripheral nervous systems, we observed reduced food intake along with a slight increase in O_2 consumption during the light phase. These observations support the idea that brain-specific Gpr75 deletion may modestly affect energy expenditure. However, reduced food intake remained the dominant factor in both models. These distinctions underscore the central role of GPR75 in appetite control and suggest that multiple brain cell types may contribute to its effects on systemic metabolism.

In contrast, *hGpr75*^{AKO} mice were not protected from HFD-induced obesity or metabolic deterioration, indicating that GPR75 signaling in adipocytes plays a minimal role in weight regulation under HFD conditions. Under acute cold exposure, these mice maintained higher core body temperatures and showed increased O_2 consumption in BAT explants, suggesting enhanced mitochondrial thermogenic capacity. However, these effects were modest and transient and did not result in systemic metabolic improvements. Thermogenic gene expression in WAT was unchanged. These findings raise the possibility that adipocyte GPR75 contributes weakly to thermogenic responses under acute stress but does not play a major role in energy homeostasis during chronic metabolic challenge.

Depot-specific effects further illustrate the complexity of GPR75 function. Prior studies reported stronger effects in WAT than in BAT (*8*). This is consistent with our finding of reduced gWAT mass in global KO mice. However, brain-specific KO mice showed an increase in gWAT mass, likely reflecting altered central control of fat distribution. Adipocyte-specific KO mice displayed increased mitochondrial activity in BAT activity but no changes in WAT mass. These results suggest that GPR75 may act differently in distinct adipose depots, potentially through both direct local and central pathways.

At the molecular level, GPR75 is known to couple to the G_q-mediated pathway, which leads to intracellular calcium flux (*27*–*30*) and downstream activation of metabolic targets. This cascade may influence both central appetite-regulating circuits and peripheral tissues such as adipose tissue. The proposed endogenous ligand 20-HETE has been linked to metabolic control (*31*, *32*), although its physiological relevance and interaction with GPR75 remain unclear (*33*, *34*). Additional studies are needed to identify endogenous ligands and clarify their effects on GPR75 function in different tissues.

Our findings are consistent with the growing body of evidence implicating G_q-coupled GPCRs in energy regulation. For example, neurokinin 2 receptor (NK2R, also known as TACR2) regulates food intake and energy expenditure through hypothalamic signaling. The G_q-coupled α-1A adrenergic receptor (ADRA1A) has also been known to enhance thermogenesis in adipocytes by increasing mitochondrial gene expression. These parallels support the role of GPR75 in modulating both central and peripheral components of energy balance and reinforce therapeutic potential of targeting this receptor class.

Downloaded from https://www.science.org at University of Texas Southwestern Medical Center on January 24, 2026

From a translational perspective, GPR75 represents a promising target for the treatment of obesity and metabolic disorders. Inhibiting GPR75 selectively in the brain could reduce appetite and modestly increase energy expenditure, offering a dual mechanism for managing body weight. However, achieving tissue-selective modulation of GPR75 without off-target effects remains a substantial challenge and will require further advances in ligand discovery and drug development. The conserved expression of GPR75 across species and tissues also suggests a possible evolutionary role in adapting to environmental stress, such as food scarcity or cold exposure. Investigating this hypothesis may provide additional insights into its physiological importance.

Future studies should include long-term metabolic assessments under varied environmental conditions, including different diet compositions and ambient temperatures. High-resolution tools such as single-cell RNA sequencing and spatial transcriptomics will be essential to uncover the cellular and molecular basis of GPR75 function in energy balance. Addressing these questions will help advance the development of targeted therapies for metabolic disease and support precision medicine approaches for obesity and related conditions.

MATERIALS AND METHODS

Study design

The aim of this study is to assess tissue-specific roles of GPR75 in metabolism. Conditional deletions were performed in the brain and adipose tissue. Brain-specific KO mice were evaluated for diet-induced obesity, food intake, and energy expenditure. Adipocyte-specific KOs were tested for systemic metabolism and BAT mitochondrial activity under cold exposure. Gpr75 expression changes under HFD were performed in brain and adipose tissue. Investigators were not blinded to genotyping or treatment groups at Touchstone Diabetes Center, Dallas, Texas, USA. Mice were maintained, and studies were performed according to protocols approved by the Institutional Animal Care and Use Committee (IACUC) of the University of Texas Southwestern Medical Center (UTSW). Mice had ad libitum access to standard or special diets, and all experiments were replicated at least once to ensure biological reproducibility and adequate statistical analysis for comparisons.

Study approval and animal housing

All animal procedures were approved by the IACUC of the UTSW Medical Center (APN 2016-101841-G). Nestin-Cre mice (strain no.003771) and adiponectin-Cre mice (strain no. 028020) were obtained from the Jackson Laboratory. All mice were housed under standard laboratory conditions (12-hour light/12-hour dark cycle) and provided with ad libitum access to food and water. Where indicated, mice were fed an HFD (60% calories from fat; Bio-Serv, catalog no. S1850).

Multiplexed error-robust fluorescence in situ hybridization

Fresh frozen mouse brains were collected immediately postmortem and snap-frozen in liquid nitrogen to preserve RNA integrity. The frozen brains were shipped on dry ice to Vizgen Inc., where they were embedded in optimal cutting temperature compound and cryosectioned at 10 μm thickness. Following sectioning, tissue samples were mounted onto MERSCOPE slides and fixed using 4% paraformaldehyde in phosphate-buffered saline (PBS) for 15 min at room temperature. Fixed slides were then returned to Eli Lilly (Boston) for downstream MERFISH sample preparation and imaging. Upon receipt, tissue sections were permeabilized overnight in 70% ethanol at 4°C. Autofluorescence quenching was not required. Encoding probe hybridization was performed using Vizgen's MERSCOPE 1000-Plex Custom Gene Panel Mix, followed by posthybridization washes with formamide wash buffer. Samples were embedded in gel using gel embedding premix and polymerized under a gel coverslip. Clearing was performed using clearing solution containing proteinase K at 47°C for 24 hours, after which samples were imaged using the MERSCOPE instrument according to the manufacturer's protocols.

Cell count quantification on MERFISH

Regions of interest (ROIs) were drawn around either the DVC (two sections) or the hypothalamus (four sections) within the Vizgen Vizualizer Software, and the cells within the ROIs were saved as a custom cell group enabling the export of the cell data as H5ad files for analysis. Quantification of $Gpr75^+$ and $marker^+$ cells was performed by classifying cells as positive if they expressed one or more transcript based on raw count data. For each marker, we calculated the proportion of $marker^+$ cells within the $Gpr75^+$ population [P ($marker^+$ | $Gpr75^+$)] and the reciprocal probability [P ($Gpr75^+$ | $marker^+$)] to assess coexpression patterns.

Generation of the floxed humanized *Gpr75* mouse line

hGpr75$^{fl/fl}$ mice were generated using CRISPR-Cas9–based genome editing. Two guide RNA sequences [CTGTATTAGACCTTGTAACA-(TGG);CCCCTTCAGAATACCAACAG-(AGG)] were designed in silico using CRISPOR (www.crispor.tefor.net) to target sequences flanking the mouse *Gpr75* ORF, upstream in the preceding intron and downstream in the 3′ UTR. A donor plasmid containing 800–base pair (bp) homology arms and a loxP-flanked version of the human *GPR75* ORF was synthetized by Genewiz (annotated sequence provided in the Supplementary Materials). Of note, only the ORF but not the UTRs of the gene were exchanged. Alt-R CRISPR-Cas9 CRISPR RNA (crRNA) guides, trans-activating CRISPR RNA (tracrRNA), and Cas9 protein (all from IDT) were mixed with circular, double-stranded plasmid donor and used for pronuclear injection into fertilized C57BL/6J eggs by the UTSW Transgenic Core. Injected eggs were transplanted into foster mothers, and the obtained offspring was screened for site-specific integration of the *hGpr75*^{flox} transgene by standard PCR. Candidate mice with apparent site-specific integration of the *hGpr75*^{flox} transgene were crossed to C57BL/6J mice. The offspring obtained from these crosses was genotyped by PCR, and the full sequence of the integrated *hGpr75*^{flfl} transgene as well as upstream and downstream regions was verified by Sanger sequencing. Fully sequence-verified mice were crossed to C57BL/6J mice for at least two more generations. We used the following primers for routine genotyping of the *hGpr75*$^{fl/fl}$ (351 bp) and nonmodified (156 bp) alleles: G481 5′-CAGCTCAGGCTTCGTCATCA-3′; G482 5′-GCAAGTGTAAAGCTGGTCGC-3′; G483 5′-GTGTGTTTCCATTGCCTGGTT-3′; and G484 5′-CTGAAGGTGGCCTGTTGAGT-3′. The KO allele (692 bp) was detected using the following primers: G483 5′-GTGTGTTTCCATTGCCTGGTT-3′ and S209 5′-CCCGTCTTCCACAAACAAACTG-3′.

Detection and quantification of *Gpr75* transcripts in brain tissues

RNA ISH was performed on tissue sections using the RNAscope Multiplex Fluorescent V2 Assay (Advanced Cell Diagnostics, catalog

Downloaded from https://www.science.org at University of Texas Southwestern Medical Center on January 24, 2026

no. 323100) to simultaneously visualize up to four different mRNAs using target specific probes, including human *GPR75* (Advanced Cell Diagnostics, catalog no. 253158-C1), mouse *Gpr75* (Advanced Cell Diagnostics, catalog no. 318281-C1), rat *Gpr75* (Advanced Cell Diagnostics, catalog no.1134291-C1), and monkey *GPR75* (Advanced Cell Diagnostics, catalog no.1072301-C1). For fluorescence ISH (fig. S4), sections were counterstained with 4′,6-diamidino-2-phenylindole, and coverslipped using a fluorescence mounting medium. Slides are scanned under a 20× objective in an Olympus VS-120 slide scanner with appropriate fluorescent filters. Target mRNA expression was evaluated quantitatively using Visiopharm software. For nonfluorescence ISH (Fig. 1), sections were counterstained with hematoxylin and coverslipped. The slides were scanned under a 20× objective in ScanScope AT slide scanner (Aperio).

Body composition analysis

Body composition was assessed using a minispec mq10 instrument (Bruker).

Physiological assays and circulating factor measurements

Oral glucose tolerance tests (oGTTs) were conducted following overnight fasting at 1.5 g/kg body weight glucose. Intraperitoneal insulin tolerance tests (ipITTs) were conducted following a 4-hour fast at 0.5 U/kg body weight insulin (Humulin R U-100, Eli Lilly). Blood glucose levels were measured using a Contour Next glucometer (Ascensia Diabetes Care) and serum insulin levels using a Mouse Ultrasensitive Insulin ELISA (enzyme-linked immunosorbent assay) (ALPCO, catalog no. 80-INSMSU-E01). oTGC tests were conducted following overnight fasting with application of 15 ml/kg body weight Intralipid (Sigma-Aldrich, catalog no. I141). Serum TG levels were determined using Infinity Triglycerides Liquid Stable Reagent (Thermo Fisher Scientific, catalog no. TR22421), serum NEFA using HR Series NEFA-HR (*2*) (Fujifilm, catalog no. 995-34791), and serum glycerol using Free Glycerol Reagent (Sigma-Aldrich, catalog no. F6428-40ML).

Metabolic cage studies

Metabolic cage studies were conducted at the UTSW Metabolic Core Facility. Mice were maintained on a 12-hour light/12-hour dark cycle at room temperature or under cold conditions as specified. Prior to the experiments, the mice were acclimated to the metabolic chambers for 5 days. Key metabolic parameters, including oxygen consumption, carbon dioxide production, food intake, and water consumption were continuously monitored and recorded using the TSE Calorimetric System (TSE Systems). Throughout the study, all transgenic mice and their littermate controls were individually housed in the metabolic chambers with ad libitum access to HFD and water.

Histological analysis

Tissues were fixed overnight at room temperature in 10% neutral-buffered formalin and thereafter stored in 50% ethanol. Fixed tissues were dehydrated, embedded in paraffin, and cut into 4- to 7-μm sections. H&E staining of deparaffinated sections was carried out according to established protocols.

RNA isolation and RT-qPCR

Tissue samples were lysed at 4°C in TRIzol (Thermo Fisher Scientific, catalog no. 15596018), and RNA was isolated using the RNeasy Mini Kit (QIAGEN, catalog no. 74106). RNA concentrations were determined on a NanoPhotometer (Implen), and cDNA synthesis was carried out using the PrimeScript 1st strand cDNA Synthesis Kit (Takara, catalog no. 6110A). RT-qPCR was performed using PowerUp SYBR Green Master Mix (Thermo Fisher Scientific, catalog no. A25778) on QuantStudio 6 Flex Real-Time PCR System (Thermo Fisher Scientific). Gene expression was normalized to the indicated housekeeping gene using the ΔΔCT method. PCR specificity was confirmed by melting curve analysis. Primer sequences are listed in table S1.

Cold exposure

For cold exposure experiments, mice were housed individually at 6°C in temperature-controlled chambers at the UTSW animal facility. During acute cold exposure, mice were housed with or without access to food for a maximum of 6 hours, with ad libitum access to water. During chronic cold exposure, mice were housed with ad libitum access to both food and water. Prior to the experiments, the mice were acclimated to the temperature-controlled chambers at room temperature for at least 1 week.

Body temperature measurement

Mice were anesthetized using isoflurane, and IPTT-300 Implantable Programmable Temperature Transponders (BMDS/Avidity Science) were embedded subcutaneously in the interscapular region. Following a 1-week recovery period, the mice were exposed to cold conditions as specified. Body temperature was monitored using a DAS-8027IUS Reader (BMDS/Avidity Science).

Isolation of adipocytes

Inguinal (gonadal) fat pads and BAT from both AKO and control mice were harvested and digested at 37°C for 45 to 60 min in a digestion buffer (1.5% bovine serum albumin) containing collagenase D (Roche, 11088866001) for WAT and collagenase B (Roche, 11088815001) for BAT. After complete digestion, 10 ml of PBS [2% fetal bovine serum (FBS)] was added to prevent collagenase activity. The cell suspension was then filtered through a 100-μm cell strainer and centrifuged at 600*g* for 5 min. The floating top layer containing mature adipocytes was collected, washed once with PBS (2% FBS), and used for RNA extraction.

Oxygen consumption experiments

Mitochondrial respiration was assessed using the Seahorse XF24 Extracellular Flux Analyzer (Agilent) according to the manufacturer's guidelines. In brief, mitochondrial respiration was measured following the recommended BOFA [basal–oligomycin–carbonyl cyanide *p*-trifluoromethoxyphenylhydrazone (FCCP)–antimycin A/rotenone] protocol. Ex vivo mitochondrial functions were evaluated using 1 to 2 mg of brown fat tissue and 4 to 5 mg of white adipocytes, respectively. For tissues, the following compounds were administered: 6-n-octylaminouracil (6-OAU, 50 μM), oligomycin (2 μM), FCCP (8 μM), and a combination of antimycin A (10 μM) and rotenone (3 μM). OCR was recorded via the Seahorse instrument.

Quantification and statistical analysis

All data are presented as means ± SEM. Statistical analyses were performed using Prism software (version 10.0, GraphPad) or Microsoft Excel. Comparisons between two independent groups were conducted using two-tailed Student's *t* tests, while one-way or two-way analyses of variance (ANOVAs) were used for multiple group comparisons.

Downloaded from https://www.science.org at University of Texas Southwestern Medical Center on January 24, 2026

A P value of less than 0.05 was considered statistically significant ($^{*}P < 0.05$; $^{**}P < 0.01$; $^{***}P < 0.001$; $^{****}P < 0.0001$). Mice were randomly grouped based on genotype, littermate status, and ear punch numbers.

Supplementary Materials

This PDF file includes:

Figs. S1 to S9
Table S1

REFERENCES

1. N. J. Pillon, R. J. F. Loos, S. M. Marshall, J. R. Zierath, Metabolic consequences of obesity and type 2 diabetes: Balancing genes and environment for personalized care. *Cell* **184**, 1530–1544 (2021).
2. N. Stefan, A. L. Birkenfeld, M. B. Schulze, Global pandemics interconnected—Obesity, impaired metabolic health and COVID-19. *Nat. Rev. Endocrinol.* **17**, 135–149 (2021).
3. X. Wen, B. Zhang, B. Wu, H. Xiao, Z. Li, R. Li, X. Xu, T. Li, Signaling pathways in obesity: Mechanisms and therapeutic interventions. *Signal Transduct. Target. Ther.* **7**, 298 (2022).
4. M. Y. Ang, F. Takeuchi, N. Kato, Deciphering the genetic landscape of obesity: A data-driven approach to identifying plausible causal genes and therapeutic targets. *J. Hum. Genet.* **68**, 823–833 (2023).
5. R. J. F. Loos, G. S. H. Yeo, The genetics of obesity: From discovery to biology. *Nat. Rev. Genet.* **23**, 120–133 (2022).
6. S. Jain, A. K. Shukla, An orphan to the rescue of obesity and steatotic liver? *Trends Endocrinol. Metab.* **35**, 761–762 (2024).
7. P. Akbari, A. Gilani, O. Sosina, J. A. Kosmicki, L. Khrimian, Y. Y. Fang, T. Persaud, V. Garcia, D. Sun, A. Li, J. Mbatchou, A. E. Locke, C. Benner, N. Verweij, N. Lin, S. Hossain, K. Agostinucci, J. V. Pascale, E. Dirice, M. Dunn, C. Regeneron Genetics, E. H. R. C. Discov, W. E. Kraus, S. H. Shah, Y. I. Chen, J. I. Rotter, D. J. Rader, O. Melander, C. D. Still, T. Mirshahi, D. J. Carey, J. Berumen-Campos, P. Kuri-Morales, J. Alegre-Diaz, J. M. Torres, J. R. Emberson, R. Collins, S. Balasubramanian, A. Hawes, M. Jones, B. Zambrowicz, A. J. Murphy, C. Paulding, G. Coppola, J. D. Overton, J. G. Reid, A. R. Shuldiner, M. Cantor, H. M. Kang, G. R. Abecasis, K. Karalis, A. N. Economides, J. Marchini, G. D. Yancopoulos, M. W. Sleeman, J. Altarejos, G. Della Gatta, R. Tapia-Conyer, M. L. Schwartzman, A. Baras, M. A. R. Ferreira, L. A. Lotta, Sequencing of 640,000 exomes identifies GPR75 variants associated with protection from obesity. *Science* **373**, eabf8683 (2021).
8. A. Leeson-Payne, J. Iyinikkel, C. Malcolm, B. Y. H. Lam, N. Sommer, G. K. C. Dowsett, P. B. Martinez de Morentin, D. Thompson, A. Mackenzie, R. Chianese, K. Kentistou, E. J. Gardner, J. R. B. Perry, F. Grassmann, J. R. Speakman, J. J. Rochford, G. S. H. Yeo, F. Murray, L. K. Heisler, Loss of GPR75 protects against non-alcoholic fatty liver disease and body fat accumulation. *Cell Metab.* **36**, 1076–1087.e4 (2024).
9. S. Hossain, A. Gilani, J. Pascale, E. Villegas, D. Diegisser, K. Agostinucci, M. M. Kulaprathazhe, E. Dirice, V. Garcia, M. L. Schwartzman, Gpr75-deficient mice are protected from high-fat diet-induced obesity. *Obesity* **31**, 1024–1037 (2023).
10. M. Chavez, A. Asthana, P. K. Jackson, Ciliary localization of GPR75 promotes fat accumulation in mice. *J. Clin. Invest.* **134**, e185059 (2024).
11. Y. Jiang, Y. Xun, Z. Zhang, Central regulation of feeding and body weight by ciliary GPR75. *J. Clin. Invest.* **134**, e182121 (2024).
12. L. Steuernagel, B. Y. H. Lam, P. Klemm, G. K. C. Dowsett, C. A. Bauder, J. A. Tadross, T. S. Hitschfeld, A. Del Rio Martin, W. Chen, A. J. de Solis, H. Fenselau, P. Davidsen, I. Cimino, S. N. Kohnke, D. Rimmington, A. P. Coll, A. Beyer, G. S. H. Yeo, J. C. Bruning, HypoMap-a unified single-cell gene expression atlas of the murine hypothalamus. *Nat. Metab.* **4**, 1402–1419 (2022).
13. V. K. Yadav, F. Oury, N. Suda, Z. W. Liu, X. B. Gao, C. Confavreux, K. C. Klemenhagen, K. F. Tanaka, J. A. Gingrich, X. E. Guo, L. H. Tecott, J. J. Mann, R. Hen, T. L. Horvath, G. Karsenty, A serotonin-dependent mechanism explains the leptin regulation of bone mass, appetite, and energy expenditure. *Cell* **138**, 976–989 (2009).
14. M. Schneeberger, L. Parolari, T. Das Banerjee, V. Bhave, P. Wang, B. Patel, T. Topilko, Z. Wu, C. H. J. Choi, X. Yu, K. Pellegrino, E. A. Engel, P. Cohen, N. Renier, J. M. Friedman, A. R. Nectow, Regulation of energy expenditure by brainstem GABA neurons. *Cell* **178**, 672–685.e12 (2019).
15. V. Garcia, A. Gilani, B. Shkolnik, V. Pandey, F. F. Zhang, R. Dakarapu, S. K. Gandham, N. R. Reddy, J. P. Graves, A. Gruzdev, D. C. Zeldin, J. H. Capdevila, J. R. Falck, M. L. Schwartzman, 20-HETE signals through G-protein-coupled receptor GPR75 (G_q) to affect vascular function and trigger hypertension. *Circ. Res.* **120**, 1776–1788 (2017).
16. Z. Ma, Y. Ning, X. Chen, S. Zhao, J. Yan, B. Wang, C. Li, R. Gao, X. Chen, N. Yang, Y. Peng, P. Li, S. Shu, 20-hydroxyeicosatetraenoic acid regulates the Src/EGFR/NF-κB signaling pathway via GPR75 to activate microglia and promote TBI in the immature brain. *Neurochem. Res.* **50**, 7 (2024).
17. M. F. Horat, S. P. Senol, O. Bahceli, M. Temiz-Resitoglu, S. Sahan-Firat, S. Sevim, B. Tunctan, Pro-inflammatory GPR75 and anti-apoptotic phospholipase signaling pathways contribute to the ameliorating effect of soluble epoxide hydrolase inhibition on chronic experimental autoimmune encephalomyelitis in mice. *Cell. Mol. Biol.* **69**, 9–16 (2023).
18. F. Tronche, C. Kellendonk, O. Kretz, P. Gass, K. Anlag, P. C. Orban, R. Bock, R. Klein, G. Schutz, Disruption of the glucocorticoid receptor gene in the nervous system results in reduced anxiety. *Nat. Genet.* **23**, 99–103 (1999).
19. G. S. Yeo, L. K. Heisler, Unraveling the brain regulation of appetite: Lessons from genetics. *Nat. Neurosci.* **15**, 1343–1349 (2012).
20. V. B. I. Johansen, J. Petersen, J. Lund, C. V. Mathiesen, H. Fenselau, C. Clemmensen, Brain control of energy homeostasis: Implications for anti-obesity pharmacotherapy. *Cell* **188**, 4178–4212 (2025).
21. J. A. Canovas, L. Wang, A. A. M. Mohamed, L. F. Abbott, C. S. Zuker, A brain center that controls consummatory responses. *Cell* **188**, 6907–6922.e17 (2025).
22. Q. Wu, M. P. Boyle, R. D. Palmiter, Loss of GABAergic signaling by AgRP neurons to the parabrachial nucleus leads to starvation. *Cell* **137**, 1225–1234 (2009).
23. C. Quarta, M. Claret, L. M. Zeltser, K. W. Williams, G. S. H. Yeo, M. H. Tschop, S. Diano, J. C. Bruning, D. Cota, POMC neuronal heterogeneity in energy balance and beyond: An integrated view. *Nat. Metab.* **3**, 299–308 (2021).
24. G. Froogh, V. Garcia, M. Laniado Schwartzman, The CYP/20-HETE/GPR75 axis in hypertension. *Adv. Pharmacol.* **94**, 1–25 (2022).
25. M. S. Vohra, K. Benchoula, C. J. Serpell, W. E. Hwa, AgRP/NPY and POMC neurons in the arcuate nucleus and their potential role in treatment of obesity. *Eur. J. Pharmacol.* **915**, 174611 (2022).
26. D. R. Powell, D. D. Doree, C. M. DaCosta, K. A. Platt, R. Brommage, L. Buhring, J. P. Revelli, M. K. Shadoan, Mice lacking *Gpr75* are hypophagic and thin. *Diabetes Metab Syndr Obes* **15**, 45–58 (2022).
27. M. Zhang, T. Chen, X. Lu, X. Lan, Z. Chen, S. Lu, G protein-coupled receptors (GPCRs): Advances in structures, mechanisms, and drug discovery. *Signal Transduct. Target. Ther.* **9**, 88 (2024).
28. J. Han, J. Li, L. Liu, K. Li, C. Zhang, Y. Han, 20-HETE mediates Ang II-induced cardiac hypertrophy via ROS and Ca^{2+} signaling in H9c2 cells. *Sci. Rep.* **15**, 2342 (2025).
29. S. Dedoni, L. A. Campbell, B. K. Harvey, V. Avdoshina, I. Mocchetti, The orphan G-protein-coupled receptor 75 signaling is activated by the chemokine CCL5. *J. Neurochem.* **146**, 526–539 (2018).
30. J. V. Pascale, E. J. Park, A. M. Adebesin, J. R. Falck, M. L. Schwartzman, V. Garcia, Uncovering the signalling, structure and function of the 20-HETE-GPR75 pairing: Identifying the chemokine CCL5 as a negative regulator of GPR75. *Br. J. Pharmacol.* **178**, 3813–3828 (2021).
31. S. Wang, S. Gao, F. Wang, Effect and mechanism of GPR75 in metabolic dysfunction-related steatosis liver disease. *Int. J. Med. Sci.* **21**, 2343–2347 (2024).
32. A. Gilani, K. Agostinucci, S. Hossain, J. V. Pascale, V. Garcia, A. M. Adebesin, J. R. Falck, M. L. Schwartzman, 20-HETE interferes with insulin signaling and contributes to obesity-driven insulin resistance. *Prostaglandins Other Lipid Mediat.* **152**, 106485 (2021).
33. F. Fan, R. J. Roman, GPR75 identified as the first 20-HETE receptor: A chemokine receptor adopted by a new family. *Circ. Res.* **120**, 1696–1698 (2017).
34. B. Tunctan, S. P. Senol, M. Temiz-Resitoglu, D. E. Yilmaz, D. S. Guden, O. Bahceli, M. F. Horat, S. Sahan-Firat, A. N. Sari, J. R. Falck, R. R. Anugu, K. U. Malik, Activation of GPR75 signaling pathway contributes to the effect of a 20-HETE mimetic, 5,14-HEDGE, to prevent hypotensive and tachycardic responses to lipopolysaccharide in a rat model of septic shock. *J. Cardiovasc. Pharmacol.* **80**, 276–293 (2022).

Acknowledgments: We thank the UTSW Transgenic Core for help in generating the *hGpr75*$^{fl/fl}$ line and the UTSW Animal Resources Center for help with mouse care. **Funding:** P.E.S. was supported by Eli Lilly and Company (SRA202207-0013). P.E.S. was supported by US National Institutes of Health grants R01-DK55758, R01-DK099110, RC2-DK118620, R01-DK127274, R01-DK131537, and P01-AG051459. D.Y.O. was supported by grants from the NIH, 5R01-DK136558. **Author contributions:** Conceptualization: D.Y.O., X.-N.S., J.-B.F., M.A., and P.E.S. Writing—original draft: D.Y.O., X.-N.S., and P.E.S. Writing—review and editing: D.Y.O., X.-N.S., J.-B.F., M.A., and P.E.S. Resources: D.Y.O., X.-N.S., M.A., and P.E.S. Funding acquisition: D.Y.O., M.A., and P.E.S. Validation: D.Y.O., X.-N.S., and P.E.S. Supervision: D.Y.O., M.A., and P.E.S. Formal analysis: D.Y.O., X.-N.S., J.S., and P.J.A. Project administration: D.Y.O. and P.E.S. Visualization: D.Y.O., X.-N.S., J.S., M.A., and P.E.S. Investigation: C.M., M.-Y.W., T.O., J.S., J.-B.F., X.-N.S., J.V., A.C., and P.J.A. Methodology: C.L., C.J., J.V., J.-B.F., J.S., P.J.A., X.-N.S., and P.E.S. Software: X.-N.S. Data curation: X.-N.S. and P.E.S. **Competing interests:** M.A., J.S, P.J.A., and C.M. are current employees of Eli Lilly & Companies. The other authors declare that they have no competing interests. **Data and materials availability:** All data and code needed to evaluate and reproduce the results in the paper are present in the paper and/or the Supplementary Materials.

Submitted 12 May 2025
Accepted 19 December 2025
Published 23 January 2026
10.1126/sciadv.ady7993

Downloaded from https://www.science.org at University of Texas Southwestern Medical Center on January 24, 2026